

Nanoscale

Accepted Manuscript



This is an *Accepted Manuscript*, which has been through the RSC Publishing peer review process and has been accepted for publication.

Accepted Manuscripts are published online shortly after acceptance, which is prior to technical editing, formatting and proof reading. This free service from RSC Publishing allows authors to make their results available to the community, in citable form, before publication of the edited article. This *Accepted Manuscript* will be replaced by the edited and formatted *Advance Article* as soon as this is available.

To cite this manuscript please use its permanent Digital Object Identifier (DOI®), which is identical for all formats of publication.

More information about *Accepted Manuscripts* can be found in the [Information for Authors](#).

Please note that technical editing may introduce minor changes to the text and/or graphics contained in the manuscript submitted by the author(s) which may alter content, and that the standard [Terms & Conditions](#) and the [ethical guidelines](#) that apply to the journal are still applicable. In no event shall the RSC be held responsible for any errors or omissions in these *Accepted Manuscript* manuscripts or any consequences arising from the use of any information contained in them.

Bi₂S₃ microspheres Grown on Graphene Sheets as low-cost counter-electrode
materials for dye-sensitized solar cells

Guang Li,¹ Xiaoshuang Chen^{2,} Guandao Gao^{3,*}*

Prof. G. Li
School of Physics and Materials Science, Anhui University
Hefei, 230601, China
liguang1971@ahu.edu.cn

Prof. X.S.Chen
National Laboratory for Infrared Physics, Shanghai Institute of Technical Physics, Chinese
Academy of Sciences, Shanghai 200083, China
E-mail: xschen@mail.sitp.ac.cn

Prof. G.D.Gao
Key Laboratory of Pollution Processes and Environmental Criteria (Ministry of Education),
Tianjin Key Laboratory of Environmental Remediation and Pollution Control,
College of Environmental Science and Engineering, Nankai University, Tianjin 300071,
China
E-mail: gaoguandao@nankai.edu.cn

Keywords: 3D Bi₂S₃ microspheres, Graphene, Counter electrode, Dye-sensitized solar cells.

Abstract

In this work, we synthesized 3D Bi₂S₃ comprised nanorods microsphere grown along (211) facet on graphene sheets by solvothermal route, and investigated its catalytic activities through I–V curves and conversion efficiency tests as CE in DSSCs. Although (211) facet has large band gap for Bi₂S₃ semiconductor, owing to the introduction of graphene into the system, its short-circuit current density, open-circuit voltage, fill factor, and efficiency were J_{sc}= 12.2 mA/cm², V_{oc}= 0.75 V, FF = 0.60, and η= 5.5%, respectively. By integrating with graphene sheets, our material achieved the conversion efficiency of 5.5%, which almost tripled the best conversion efficiency value of the DSSCs with (211) faceted 3D Bi₂S₃ without graphene conversion efficiency (1.9%) reported by the latest literature. Since this conversion-efficient 3D material grown on the graphene sheets significantly raises the catalytic property, it paves routes for designing and applying low-cost Pt-free CE materials in DSSC from inorganic nanostructures.

1. Introduction

Due to having a single-layered structure of sp²-hybridized carbon atoms, monolayer graphene displays similar electronic properties as a zero-bandgap semiconductor and thus is promising for electronic transportations and storage ^[1-2]. Various attractive properties of monolayer graphene such as its high electrical conductivity, low weight, great mechanical strength and structural flexibility make it an ideal substrate for growth and anchoring of insulating materials ^[3-5]. In fact, formation of nanostructures on graphene sheets can improve the electrochemical stability and conductivity of nanomaterials. For instance, metallic oxide nanomaterials such as Mn₃O₄, Co₃O₄, and Fe₃O₄ grown on graphene have displayed augmented specific capacities and rate capabilities, thereby raising their performances as anode materials for lithium ion batteries (LIB) ^[6-8]. In addition, recent work has shown a better storage performance of LIB using SnSe₂ nanoplate–graphene composites as anode

materials as oppose to using SnSe₂ nanoplates or graphene alone^[9]. Moreover, researchers of late have developed a porous nanoarchitecture from 2D graphene–SnS₂ (G–SnS₂) units, which endows the high-rate transportation of electrolyte ions and electrons throughout the electrode matrix, thus giving rise to promising electrochemical properties as anode materials for LIB^[10].

Bismuth sulfide (Bi₂S₃), which is a type of semiconductors with a direct band gap, endows a layered structure and crystallizes in the orthorhombic system (pbnm space group)^[11-12]. It has drawn great research attentions as it has a reasonably low band gap of 1.7eV, an absorption coefficient on the order of 10⁴ to 10⁵ cm⁻¹, and an incident photon to electron conversion efficiency of ~5%, which are suitable for PEC applications^[13]. At present, various types of Bi₂S₃ nanostructure materials such as nanowires^[14-16], nanorods^[17-18], and nanotubes^[19] have been synthesized by proper methods including colloidal chemistry routes^[14-15], hydrothermal reactions^[16-18], solvent-free syntheses^[17], solvothermal reactions^[17-20], aerosol assisted chemical vapor depositions (AACVD)^[19], and vapor position methods^[21]. The aforementioned methods raise the performances of Bi₂S₃ in photo detectors and optoelectronic type nanodevices; as well as biomolecule detectors and H₂ Sensors^[15, 16, 19].

Owing to ordered nanostructures and complex morphologies, current trends in nanoscience and nanotechnology point toward the fabrication of 3D assemblies, which show promise in catalysis, Li-ion batteries, solar cell, water treatment, etc.^[22-25] In particular, fabrications of semiconductor materials that manipulate crystal facets have drawn increasing attentions since the photoelectric properties of the semiconductors can be further enhanced for highly-economic replacement of the scarce Pt counter-electrode (CE) in Dye-sensitized solar cells (DSSCs). For example, Zhang et al. compared the catalytic activities of the (130), (211), (221) and (040) facets within Bi₂S₃ through DFT computations and experimental validations. The computations suggest that the (130) facet within Bi₂S₃ has the highest surface energy, the best electrical conductivity and the highest position of the conduction band minimum of the four facets, suggesting the most effective electron transfer path from Bi₂S₃-130 CEs to the I₃⁻.

This is further substantiated by the superiority of conversion efficiency of DSSCs with (130) faceted Bi_2S_3 CEs (3.5%) over that with (211) faceted Bi_2S_3 CEs (1.9%) [26]. Controlled organization of primary building units of Bi_2S_3 into curved structures on graphene sheets with a spherical configuration along a specific facet will further improve their electrical properties, though it remains a big challenge to grow nanocrystals on graphene sheets in solution for materials with more sophisticated compositions and structures.

Herein, we report the synthesis of 3D Bi_2S_3 comprised nanorods with microsphere morphologies on graphene sheets along a specific facet through a solvothermal route. The decomposition of L-cysteine at temperatures of 150°C allowed S^{2-} to efficiently diffuse, and graphene oxide sheets were used as a starting substrate for 3D Bi_2S_3 growth and anchoring, which were fully reduced to graphene during solution step. Its electrical properties as a counter electrode in DSSCs are also investigated. This work suggests that it is possible to grow 1D nanorods into 3D microspheres on graphene sheets through a one-step solvothermal methodology under controlled conditions.

2. Results and Discussion

The atomic force microscopy (AFM) image shown in **Figure S1** indicates the height of graphene oxide to be 0.35–1 nm, and reveals that the graphene sheets are either mono- or bilayered. **Figure 1a** shows a typical TEM image of a Bi_2S_3 nanorod-based superstructure, where microspheres are formed on graphene sheets. **Figure 1b** shows a typical transmission electron microscopy (TEM) image of an isolated Bi_2S_3 nanorod-based superstructure. The edge portion of the superstructure is lighter than that of the center, and is comprised of rod-like 1D nanostructures. The high-resolution TEM (HRTEM) image of a single nanorod in the microspheres shows the single-crystalline structure (**Figure 1c and 1d**), and the nanorods exhibit diameters of 10-15 nm and a shortest length of 250nm. The lattice spacing of 0.23 nm corresponds to the d-spacing between adjacent (211) crystallographic planes of Bi_2S_3

nanorods. The as-synthesized nanorods are elongated along the [211] direction; the lengthwise axes of the nanorods are parallel to the [211] direction, which indicates that the nanostructures indeed grow along a certain direction.

Low-magnification scanning electron microscopy (SEM) observations show that the as-obtained Bi_2S_3 samples are composed of many uniform, sphere-like architectures ranging from 0.65 to 2.5 μm in diameter (**Figure 2 a**). Higher-magnification SEM images reveal that Bi_2S_3 microspheres build from crystalline nanorods. These crystal rods, analogous to a dandelion, are aligned perpendicularly to the spherical surface, pointing toward the common center (**Figures 2b, 2c, and 2d**).

Powder X-ray diffraction (XRD) is used to characterize the phase structure of the products. It can be seen from **Figure 3** that the XRD pattern is in conformity with orthorhombic Bi_2S_3 (JCPDS: JCPDS no. 17-0320, red pattern in **Figure 3**). No characteristic peak was observed for other impurities such as Bi, S, and Bi_2O_3 . This indicates that pure crystalline Bi_2S_3 was formed via the solvothermal process. From **Figure 3**, it can also be known that (130), (211), and (040) planes show the three strongest diffraction peaks, and the relative diffraction intensity of (211)/(130) is higher than the corresponding conventional values. The resultant Bi_2S_3 products are mainly dominated by (211) facets, and therefore their (211) planes tend to be preferentially oriented parallel to the surface of the supporting substrate on graphene sheets in the experiment, which is consistent with the HRTEM analysis.

FT-IR spectra of graphene oxide (GO) and graphene supported Bi_2S_3 microspheres (G- Bi_2S_3) is shown in **Figure S2**. The three bands of GO appear at 1050 cm^{-1} , 1720 cm^{-1} , and 3450 cm^{-1} and are due to the epoxide and carboxyl functional moieties, respectively. This result clearly reveals that functional groups are introduced into carbon frameworks upon oxidation. However, in case of G- Bi_2S_3 , epoxide and carboxylate functional groups almost disappear, which confirms that GO has been reduced to graphene during the solution step, which is consistent with the XRD results (**Figure S2 and Figure 3**).

The relationship between morphologies of Bi_2S_3 and synthesis time was also investigated. The SEM images of Bi_2S_3 at different synthesis times (1, 2, 4, and 24hrs) are shown in **Figure 4a-c** and **Figure 2** respectively. After 1 hr of synthesis, irregular nanoparticles began forming on the graphene sheets. The sphere-like shapes and nanorod-comprised microsphere formation became apparent after 2 hrs, followed by the formation of clearer nanorod-comprised microspheres after 4 hrs. After 24 hrs, microspheres with narrowly distributed diameters were visible, as seen in **Figure 2**. The results reveal that reaction time is one of the main factors to form nanorod-based Bi_2S_3 microspheres with narrowly distributed diameters; that is, the Ostwald ripening process is indispensable. The formation process of Bi_2S_3 microspheres on graphene is shown in **Figure 5**.

In a control experiment, the same synthetic steps without mildly oxidized graphene oxide (mGO) being added produced nanorod-based Bi_2S_3 microspheres (See supporting information, **FigureS4**). Thus, the results suggest that mildly oxidized graphene sheets are a strong candidate for growing nanocrystals into well-defined morphologies. In this process, the functional groups on mGO allow adsorption of cations and nanoparticle nucleation to achieve uniform precursor coating in the first step of the reaction, the conjugated graphitic regions of reduced mildly oxidized graphene oxide (rmGO formed by reduction of mGO under solvothermal conditions) weakly interact with surface species to promote the formation of well-defined shapes of nanocrystals by anisotropy under reactive conditions. The resulting nanorod-based Bi_2S_3 microspheres can be bonded to rmGO by Bi-O-C bonds at the remaining oxygen sites and by Van der Waals interactions with the aromatic regions of rmGO.

By tuning the surface atomic structures, the photoelectric and photocatalytic properties of facet-controlled semiconductor materials can be further optimized for DSSC applications^[27-30]. Electronic conductivity is one of the critical factors that influence the catalytic activity of CEs in DSSCs. In semiconductors, electrical conductivity increases with decreasing band gap. The periodic density functional theory (DFT) computations performed by a slab model

revealed that the (040) facet for Bi_2S_3 crystalline has the largest band gap, and the continuing facet order from smaller to larger is $(211) > (221) > (130)$, so electrons can transfer from Bi_2S_3 facets to I_3^- in the following sequence: (130), (221), (211), (004).^[26] However, the conversion efficiency of all Bi_2S_3 3D nanoproducs needs to be improved. To enhance their electronic conductivity, it is necessary to further adjust band gap of the semiconductors.

Due to the electron transfer from the conduction band of semiconductor to the graphene^[31-32], we speculate that the electronic conductivity of semiconductors will obviously increase, which grows along a specific facet for large band gaps. So we synthesized 3D Bi_2S_3 microspheres with assembled-nanorods grown along [211] facet on graphene sheets, and investigated its photovoltaic property in DSSCs. The Bi_2S_3 sample film was fabricated by the doctor blade method on FTO conductive glass and sensitized with N719 dye. The short-circuit current density, open-circuit voltage, fill factor, and efficiency were $J_{sc} = 12.2 \text{ mA/cm}^2$, $V_{oc} = 0.75 \text{ V}$, $FF = 0.60$, and $\eta = 5.5\%$, respectively, in **figure 6**. Comparison with reference^[33], the conversion efficiency of our product has an advantage over that of Bi_2S_3 comprised nanorod-like microsphere, which grow along the same [211] facet and η of which equals 1.9%. In fact, the conversion efficiency of the Bi_2S_3 microspheres grown along [211] facet on graphene is more than that of the Bi_2S_3 microsphere grown along [130] facet, which owns the smallest band gap in reference^[26]. Because graphene is a zero-bandgap semiconductor and shows highly electronically conductive properties for storing and transporting electrons, it is possible that the conversion efficiency of synthetic Bi_2S_3 microspheres along [130] facet on graphene as a counter electrode has an advantage over that of Pt in dye-sensitized solar cells which was listed in **figure S6** as compare.

Electrical impedance spectroscopy (EIS) is effective for evaluation of the electron conductivity and mass diffusion of materials. EIS has been carried out to study the charge-transfer processes at the interface between the Bi_2S_3 electrodes and the electrolyte. We use the symmetric sandwich-like configuration to exclude the influence of the TiO_2 photoanode.

The Nyquist plots are shown in **Figure 7**, where three hemi-spheres are observed. The hemisphere in the high-frequency region represents the resistance applied to the Bi₂S₃ electrode and to the interface between FTO and Bi₂S₃ layers, while those in the intermediate and low-frequency region offer information on the resistance at the Bi₂S₃ /electrolyte interface and the finite layer Nernst diffusion impedance within the electrolyte, respectively. The equivalent circuit (shown in **Figure 8**) consisted of several components: ohmic resistance (R_s), charge transfer resistance at the FTO/ Bi₂S₃ layers (R₁, 20.1 Ω), charge transfer resistance at the photoelectrode/electrolyte (R₂, 9.2 Ω), charge transfer resistance at the finite layer (Nernst diffusion impedance) (R₃, 5.5 Ω), the constant phase element of capacitance corresponding to R₁(CPE₁), the constant phase element of capacitance corresponding to R₂(CPE₂), and the constant phase element of capacitance corresponding to R₃(CPE₃). For electrodes having a rough surface the semicircle is flattened and C_d is often replaced by a constant phase element (CPE), where CPE was defined by two parameters, CPE-p and CPE-t. Basing on the

formula: $Z = \frac{1}{T \cdot \omega^p} [\cos(\frac{-p\pi}{2}) + j \sin(\frac{-p\pi}{2})]$, when CPE-p = 1, and CPE is pure C_d, generally, CPE-p is from 0.5 to 1.0. in our model circuit, the corresponding CPE-p all is less than 1.0, which explores that the corresponding electrodes surface are rough and the ideal C_d cannot describe them correctly, resultantly, C_d needs to be modified and replaced by CPE for better explaining them. By EIS analysis, the largest impedance comes from the charge-transfer resistance (R₁, 20.1 Ω), however, the good contact between FTO/ Bi₂S₃ layers benefits to reduce the main resistance (R₁), on the other hand, both R_s and R₃ depend on ionic conductance from the electrolyte between anode and cathode. These internal impedances have a direct effect on the electron transport mechanism in DSSCs. As a consequence, the cell performance of the DSSCs is improved when the sum of the resistance components (R_s, R₁, R₂, and R₃) is small.

3. Conclusion

By introducing the graphene with outstanding carrier transfer properties, the electronic conductivity of CEs should be dramatically enhanced and the electronic transfer from CEs to triiodine could be more efficient. We developed the first synthesis of complex single-crystalline nanomaterials on highly conducting mildly oxidized graphene sheets with desired size and morphology along a specific facet. The resulting high electrical conductivity and catalytic activity led to excellent rate performance for the otherwise extremely insulating 3D Bi₂S₃ counter electrode material. This work opens the door to complex hybrid materials design and engineering with graphene for advanced energy materials for dye-sensitized solar cells.

4. Experimental Section

Synthesis of GO Nanosheets:

Graphene oxide (GO) nanosheets were made by a modified Hummers method. In detail, graphite powder (2 g) was put into 100 mL of cooled (0°C) concentrated H₂SO₄, followed by the slow addition of KMnO₄ (6 g), a slight exotherm may be produced in this process. The suspension was then allowed to stir at 35°C for 12-15 hours. Afterwards, 200 mL of distilled water was added and the temperature was kept at 96 °C for 2 hrs. The temperature was reduced to 60 °C, and 10 mL of H₂O₂ (30%, 10mL) was injected into the suspension to completely react with the excess KMnO₄ which yielded a bright yellow mixture. The solid product was separated by centrifugation, and then washed with HCl (5%) several times and with water until the pH value of the supernatant was nearly 6, and graphene oxide was obtained. The collected precipitate was dispersed in water, then sonicated and subsequently concentrated to obtain a GO suspension, and kept at 50 °C for 10 hrs and GO powder was obtained.

Synthesis of Bi₂S₃/reduced graphene oxide Hybrid:

The concentration of the final GO water suspension was 0.05g/8ml. A two-step approach for synthesis is used in this process. In the first step of synthesis, 0.1 g of GO powder was added into a 50 mL beaker with 40 mL of absolute ethanol, and then 1.0 g of $\text{Bi}(\text{NO}_3)_3$ was added stirred with a magnetic stirrer to form a homogeneous solution, then 0.8 g of L-cysteine was added. Subsequently, the mixture was transferred into a Teflon-lined stainless steel autoclave with a capacity of 50 mL for solvothermal treatment at 150 °C for 15 hrs. In the second step of synthesis, after the autoclave was allowed to cool to room temperature, 0.5 g of L-Ascorbic acid was added to the autoclave and magnetically stirred. The mixture was then sealed in the autoclave for solvothermal reaction at 150°C for another 9 hours. The precipitate was separated by centrifugation, after which it was washed with water and absolute ethanol to remove impurities, and the Bi_2S_3 /reduced graphene hybrid was obtained.

Characterization:

The phase of the samples was characterized by X-ray diffraction (XRD) under a Rigaku D/Max-2500 X-ray diffractometer employing $\text{Cu K}\alpha$ radiation, with $\lambda = 1.54056 \text{ \AA}$. The morphology and size of the samples were characterized by using a field emission scanning electron microscope (JEOL JSM-6700) and transmission electron microscopy (TEM, JEOL-2010, with an operating voltage of 200 kV), high-resolution TEM (HRTEM, JEOL-2010), AFM (Multimode8, Bruker).. The Fourier transform infrared (FT-IR) spectrum was recorded with a GX spectrophotometer (Perkin -Elmer) with the KBr wafer technique.

Photovoltaic performance tests:

Approximately 0.05 g of Bi_2S_3 powder was mixed with 0.5 mL of 2.5% PEG20000 solution and stirred until a fluid mixture formed. A film was then made using the doctor-blade method on FTO conductive glass (LOF, TEC-15, 15Wper square). The film was heated at 450 °C for 1 hr in argon atmosphere to obtain the Bi_2S_3 counter electrode. A commercial TiO_2 sol (Solaronix, Ti-Nanoxide T/SP) was used to prepare the TiO_2 film on FTO also through the doctor-blade method, and the film was soaked in an N-719 dye solution (in ethanol) for 24 hrs

to obtain dye-sensitized TiO₂ electrodes. DSSCs were assembled by injecting the electrolyte into the aperture between the dye-sensitized TiO₂ electrode and the counter electrode. The liquid electrolyte composed of 0.05 M I₂, 0.1 M LiI, 0.6 M 1,2- dimethyl-3-propylimidazolium iodide (DMPII), and 0.5 M 4- tert-butyl pyridine in acetonitrile. Surlyn 1702 was used as the separator between the two electrodes. The two electrodes were clipped together and solid paraffin was used as the sealant to prevent the electrolyte from leaking. The effective cell area was 0.25cm². Photocurrent–voltage curves were measured with a Zahner IM6ex electrochemical workstation with a Trusttech CHF-XM-500W source under simulated sun illumination (Global AM 1.5, 100 mW cm⁻²).

Supporting Information

Supporting Information is available online.

Acknowledgements

This work was financially supported by the State Key Program for Basic Research of China (No. 2013CB632705), National Natural Science Foundation of China (Nos. 61290301 and 11174002), and “211 Project” of Anhui University.

Received: ((will be filled in by the editorial staff))

Revised: ((will be filled in by the editorial staff))

Published online: ((will be filled in by the editorial staff))

- [1] M. J. Allen, V. C. Tung, R. B. Kaner, *Chem. Rev.* **2010**, *110*, 132.
- [2] C. N. R. Rao, A. K. Sood, K. S. Subrahmanyam, A. Govindaraj, *Angew. Chem., Int. Ed.* **2009**, *48*, 7752.
- [3] S. Park, R. S. Ruoff, *Nat. Nanotechnol.* **2009**, *4*, 217.
- [4] H. Wang, J. T. Robinson, G. Diankov, H. Dai, *J. Am. Chem. Soc.* **2010**, *132*, 3270.
- [5] H. L. Wang, Y. Yang, Y. Y. Liang, L. F. Cui, H. S. Casalongue, Y. G. Li, G. S. Hong, Y. Cui, H. J. Dai, *Angew. Chem. Int. Ed.* **2011**, *50*, 7364.
- [6] H. Wang, L. Cui, Y. Yang, H. S. Casalongue, J. T. Robinson, Y. Liang, Y. Cui, H. Dai, *J. Am. Chem. Soc.* **2010**, *132*, 13978.
- [7] S. Yang, G. Cui, S. Pang, Q. Cao, U. Kolb, X. Feng, J. Maier, K. Mullen, *ChemSusChem.* **2010**, *3*, 236.
- [8] M. Zhang, D. Lei, X. Yin, L. Chen, Q. Li, Y. Wang, T. Wang, *J. Mater. Chem.* **2010**, *20*, 5538.
- [9] J. Choi, J. Jin, I. G. Jung, J. M. Kim, H. J. Kim, S. U. Son, *Chem. Commun.* **2011**, *47*, 5241.
- [10] B. Luo, Y. Fang, B. Wang, J. S. Zhou, H. S. Song, L. J. Zhi, *Energy Environ. Sci.* **2012**, *5*, 5226.
- [11] Y. Yu, C. H. Jin, R. H. Wang, Q. Chen, L. M. Peng, *J. Phys. Chem. B.* **2005**, *109*, 18772.
- [12] Y. Yu, R. H. Wang, Q. Chen, L. M. Peng, *J. Phys. Chem. B.* **2006**, *110*, 13415.
- [13] L. M. Peter, K. G. U. Wijayantha, D. J. Riley, J. P. Waggett, *J. Phys. Chem. B.* **2003**, *107*, 8378.
- [14] O. W. Thomson, L. Cademartiri, M. MacDonald, S. Petrov, G. Calestani, P. Zhang, G. A. Ozin, *J. Am. Chem. Soc.* **2010**, *132*, 9058.
- [15] L. Cademartiri, F. Scotognella, P. G. O'Brien, B. V. Lotsch, J. Thomson, S. Petrov, N. P. Kherani, G. A. Ozin, *Nano Letters.* **2009**, *9*, 1482.

- [16] K. Yao, W. W. Gong, Y. F. Hu, X. L. Liang, Q. Chen, L. M. Peng, *J. Phys. Chem. C* **2008**, *112*, 8721.
- [17] Y. Wang, J. Chen, P. Wang, L. Chen, Y. B. Chen, L. M. Wu, *J. Phys. Chem. C* **2009**, *113*, 16009.
- [18] Q. F. Han, J. Chen, X. J. Yang, L. D. Lu, X. Wang, *J. Phys. Chem. C* **2007**, *111*, 14072.
- [19] A. A. Tahir, M. A. Ehsan, M. Mazhar, K. G. U. Wijayantha, M. Zeller, A. D. Hunter, *Chem. Mater.* **2010**, *22*, 5084.
- [20] W. Lou, M. Chen, X. Wang, W. Liu, *Chem. Mater.* **2007**, *19*, 872.
- [21] X. Yu, C. Cao, *Cryst. Growth Des.* **2008**, *8*, 3951.
- [22] M. Ge, Y. F. Li, L. Liu, Z. Zhou, W. Chen, *J. Phys. Chem. C* **2011**, *115*: 5220.
- [23] C. S. Guo, M. Ge, L. Liu, G. D. Gao, Y. C. Feng, Y. Q. Wang, *Environ. Sci. Technol.* **2010**, *44*, 419.
- [24] L. Gur, N. A. Fromer, C. P. Chen, A. G. Kanaras, A. P. Alivisatos, *Nano Lett.* **2007**, *7*, 409.
- [25] L. Liu, Y. Li, S. M. Yuan, M. Ge, M. M. Ren, C. S. Sun, Z. Zhou, *J. Phys. Chem. C* **2010**, *114*, 251.
- [26] H. J. Zhang, L. T. Yang, Z. Liu; M. Ge, Z. Zhou, W. Chen, Q. Z. Li, L. Liu, *J. Mater. Chem.* **2012**, *22*, 18572.
- [27]. A. M. Claren, T. Valdes-Solis, G. Li, S. C. Tsang, *J. Am. Chem. Soc.* **2009**, *131*, 12540.
- [28]. S. Liu, J. Yu, M. Jaroniec, *J. Am. Chem. Soc.* **2010**, *132*, 11914.
- [29]. S. Choi, K. An, E. Kim, J. Yu, J. Kim, T. Hyeon, *Adv. Funct. Mater.* **2009**, *19*, 1645.
- [30]. G. Li, N. Dimitrijevic, L. Chen, J. Nichols, T. Rajh, K. A. Gray, *J. Am. Chem. Soc.* **2008**, *130*, 5402.
- [31] S. Stankovich, D. A. Dikin, G. H. B. Dommett, K. M. Kohlhaas, E. J. Zimney, E. A. Stach, R. D. , Piner, S. T. Nguyen, R. S. Ruoff, *Nature*. **2006**, *442*, 282.
- [32] H. Zhang, X. Lv, Y. Li, Y. Wang, J. Li, *ACS Nano*. **2010**, *4*, 380.
- [33] J. F. Wang, Z. Liu, S.M. Yuan, L. Liu, Z. Zhou, W. Chen, *Aust. J. Chem.* **2012**, *65*, 1342.

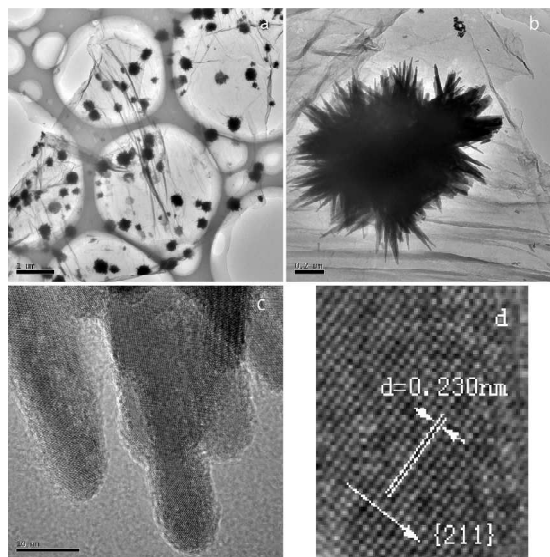


Figure 1: TEM images of Bi_2S_3 sample

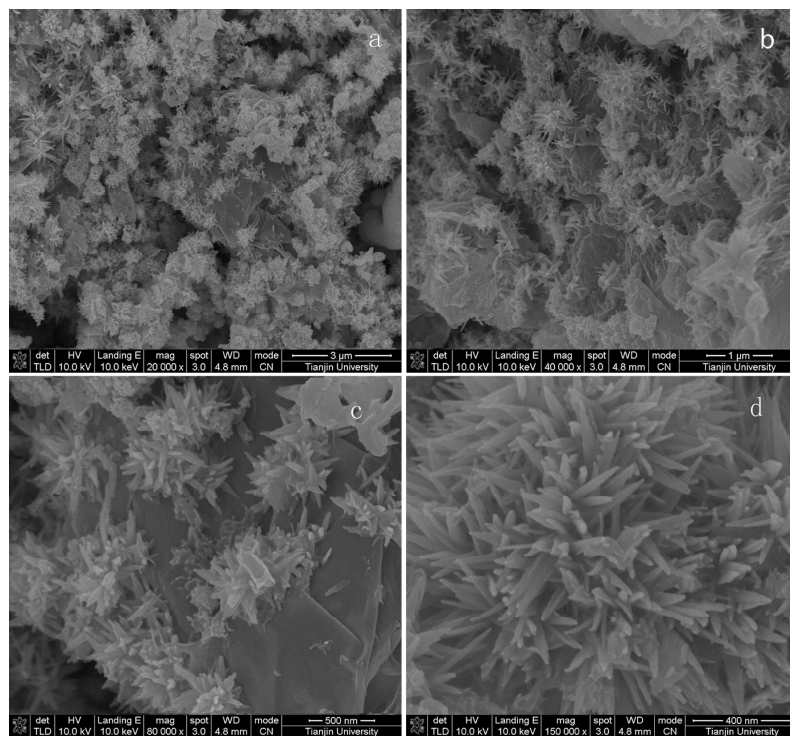


Figure 2: SEM images of the Bi_2S_3 sample

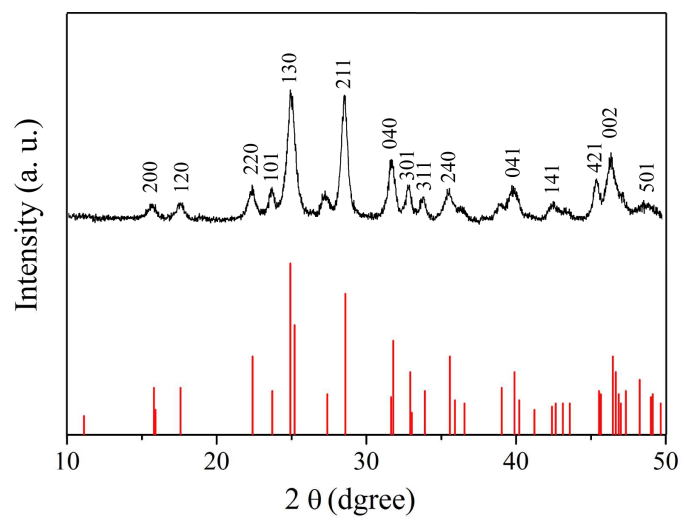


Figure 3: XRD pattern of the Bi_2S_3 sample

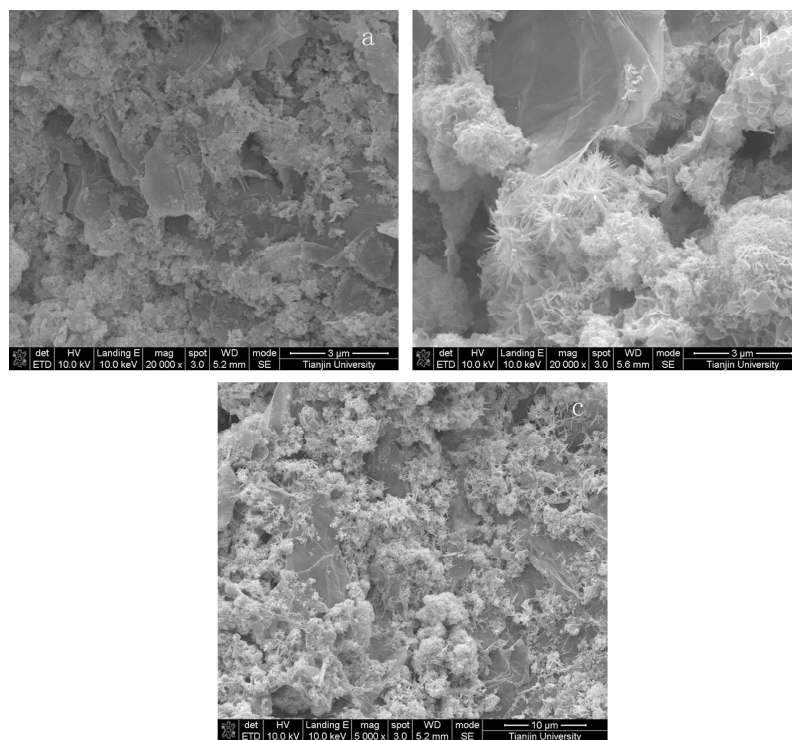


Figure 4: SEM images of different synthetic time, a: 1hr, b: 2hrs, c: 4hrs.

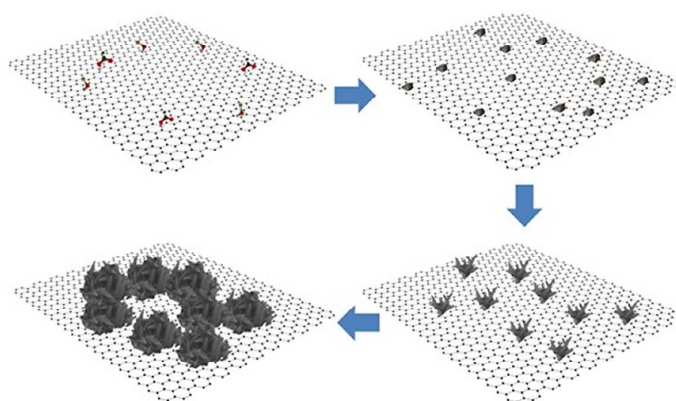


Figure 5: The formation process of the Bi₂S₃ microspheres

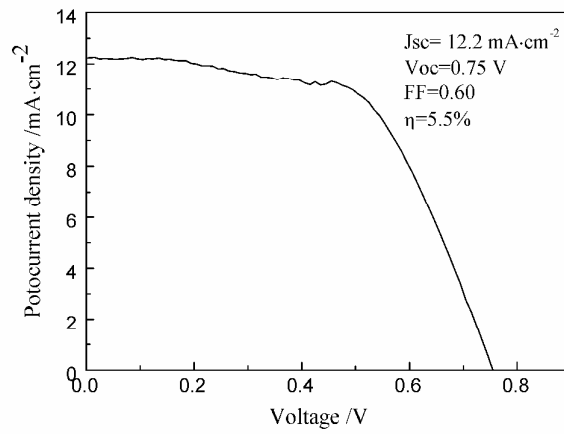


Figure 6: I-V curve of Bi_2S_3 sample

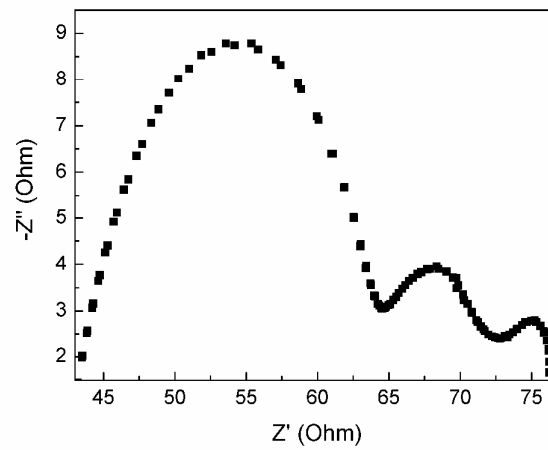


Figure 7: Nyquist plots of measured EIS spectra of the counter electrode

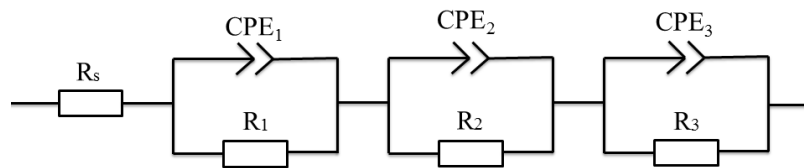
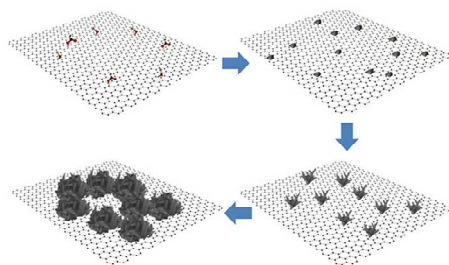


Figure 8: Equivalent circuit of the symmetric device

Table 1. Simulation value of equivalent circuit of the figure.8

Rs	43.68
R1	20.1
CPE1-t	3.65E-06
CPE1-p	0.89775
R2	9.2
CPE2-t	0.0015329
CPE2-p	0.74425
R3	5.5
CPE3-t	0.09454
CPE3-p	0.81824

Graphical Abstract:

3D Bi₂S₃ microspheres with nanorods-assembled grown along (211) facet on graphene sheets were synthesized with obviously enhanced CEs.